Progress In Electromagnetics Research C, Vol. 69, 27–36, 2016

Compact Broadband Circularly Polarized Monopole Antenna for Global Navigation Satellite System (GNSS) Applications

Ke Wang, Hongyan Tang*, Runmiao Wu, and Chao Yu

Abstract—A compact monopole antenna with broadband circular polarization for global navigation satellite system (GNSS) applications is presented in this paper. The proposed antenna comprises a simple tilted radiator fed by 50-Ohm microstrip line and an improved ground plane. By embedding two isosceles right triangular slits and introducing an isosceles right triangular perturbation in the ground plane, the circularly polarized (CP) performance can be improved significantly. The impedance and circular polarization characteristics are studied by simulation and measurement. With a compact size of $79 \times 79 \times 1.5\,\text{mm}^3$ for the fabricated antenna, a measured 10-dB return loss bandwidth of 35.6% (1.13–1.62 GHz) and a 3-dB AR bandwidth of 35.4% (1.14–1.63 GHz) can be achieved.

1. INTRODUCTION

In recent years, the Global Navigation Satellite System (GNSS) has been increasingly investigated for military and civilian research fields, which accelerates the development of terminal antennas. The GNSS, which includes BEIDOU Navigation Satellite System (BEIDOU) of China, Global Positioning System (GPS) of the USA, Galileo Navigation Satellite System (GALILEO) of Europe, and Global Navigation Satellite System (GLONASS) of Russia, is a global service to provide the precise time, velocity, and position for moving objects. GNSS spectrum covers 0.470 GHz from 1146 to 1616 GHz. In satellite navigation field, the design of GNSS antennas with compact size, multiple or wide operation bands, and right-hand circular polarization (RHCP) for the receivers on ships, air planes, or mobile terminals, has become a hot research area [1].

In previous studies [2, 16], different kinds of circularly polarized (CP) antennas were presented for the GNSS applications. Some of the utilized techniques include using serial feeding network [2], parasitic shorting strips [3], arc-shaped structure array [4], capacitive feeding disks and arc-shaped slots [5], orthogonally located slots [6], a high impedance surface ground under an annular slot patch [7], two radiating polygon loops [8], concentric annular-ring patch [9], dual-feed configuration and 90° phase shifter feed network [10], incorporating a proximity-coupled feed [11], cross-type traveling wave strip [12], and three stacked layers of rectangular patches [13]. In [14], a GPS reception antenna with small size and low profile was developed for multifunctional handsets by introducing a compact coupled feed network at the corner of the printed-circuit board. In [15], a novel folded patch antenna was proposed for the vehicle GPS tracker. In [16], a novel dual-band antenna was realized by using a modified annular ring and a square patch for GPS and satellite digital audio radio (SDARS) automotive applications. However, the CP antennas mentioned above were characterized by single operation band [24], large frequency ratio for dual-band antenna [5, 6], narrow 3-dB axial-ratio (AR) bandwidth [7, 8], complex techniques [9–11] or non-planar structure [12, 13], respectively.

Received 11 August 2016, Accepted 11 October 2016, Scheduled 27 October 2016
* Corresponding author: Hongyan Tang (hytang@uestc.edu.cn).
The authors are with the School of Electronic Engineering, University of Electronic Science and Technology of China, Chengdu, Sichuan 610054, People's Republic of China.

By literature review, a number of techniques for obtaining wideband CP antennas have been reported [17, 22]. In [17], a novel broadband CP patch antenna for GPS applications was achieved by introducing four-output feed network so that the ring slot patch can produce circular polarization The four parasitic arc-shaped patches helped to achieve a wide 3-dB AR bandwidth of 16% (1.51–1.77 GHz). A compact broadband CP patch antenna for Global star and GPS applications was reported in [18] where the 90° hybrid was used to produce the dual circular polarization. It achieved a 3-dB AR bandwidth of 5% (1.57–1.65 GHz). In [19], a wideband CP antenna based on cavity-backed slot for GNSS applications was designed. A wideband CP antenna with four radiating arms and two Wilkinson power dividers was proposed in [20]. It yielded a 3-dB AR bandwidth of 23.5% (1.50–1.90 GHz). In [21], multipath effect was reduced by employing a choke ring and broadband circular polarization was obtained by introducing a specific feed network and an L-probe feed. The antenna obtained a 3-dB AR bandwidth of 30.6% (1.19–1.62 GHz). In [22], a single straight feed-line and annular slot patch with diagonal slots were proposed. By appropriately varying the iteration order and iteration factor of fractal elements a 3-dB AR bandwidth of 21.8% (1.47–1.83 GHz) was accomplished. However, these broadband CP antennas have larger size of more than $100 \times 100\,\text{mm}^2$ [17–19], complex structure [21, 22], or higher loss at the feed network due to the resistors [20]. From these instances, it can be seen that designing a broadband CP antenna with desired operating frequency band, compact size, and good CP performance is still a challenge for antenna designers.

This paper demonstrates a compact monopole antenna with broadband circular polarization. In order to realize the objective of wide CP bandwidth and compact size, an improved ground plane is introduced and a simple tilted radiating patch is designed. The proposed antenna is fabricated and tested. Measured results indicate that the 10-dB return loss bandwidth is 35.6% (1.13–1.62 GHz), and the 3-dB AR bandwidth is 35.4% (1.14–1.63 GHz). The results of simulation and measurement have a good agreement. Detailed geometry of the proposed design, parametric study, and measure results are presented and discussed. The proposed antenna has great potential for the application of GNSS systems.

2. ANTENNA DESIGN AND ANALYSIS

2.1. Antenna Design

Figure 1 illustrates the geometry of the proposed broadband CP monopole antenna. The proposed antenna consists of an improved ground plane and a simple radiator. They are built on the FR4 dielectric substrate with a dielectric constant of 4.4 and a loss tangent of 0.02. The overall size of the

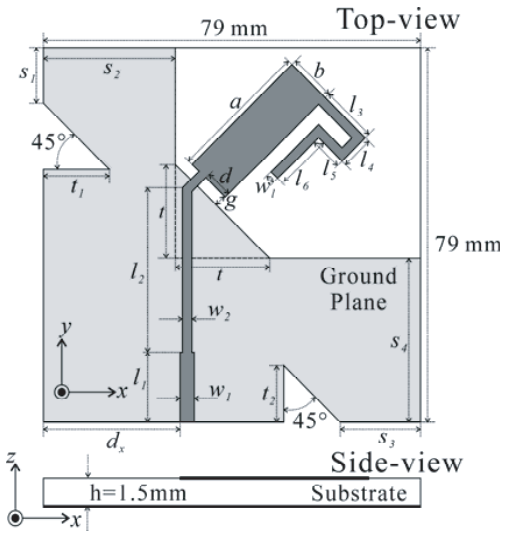

Figure 1. Geometry of the proposed broadband monopole antenna.

Table 1. Dimensions of the propose antenna (unit: mm).

parameter	*value*	*parameter*	*value*	*parameter*	*value*
a	35	b	10.2	d_x	27.9
l_1	15	w_1	3	l_2	34.6
w_2	2.5	d	4.9	g	2.7
l_3	10.2	l_4	5.5	l_5	6.2
l_6	11	w_l	2	t	19.5
t_1	13.3	t_2	19.5	s_1	12.3
s_2	26.1	s_3	10	s_4	33.4

antenna is $79 \times 79 \times 1.5\text{mm}^3$. The radiating patch is asymmetrically fed by a 50-Ohm microstrip line with width of w_1 and length of l_1. An impedance transformer with width of w_2 and length l_2 is used to match the impedance between the 50-Ohm feed line and the radiator. Typically, the monopole antenna is either horizontal or vertical linearly polarized. By rotating the radiator 45° around the vertical axis and introducing the asymmetrical feed structure, two orthogonal resonant modes with equal amplitude and 90° phase difference are generated, thus CP radiation can be excited. From the conventional method for monopole antenna design, the length of the radiator is about quarter wave length. To reduce the size of the proposed antenna, two L-shaped strips are added to the rectangular patch, and the total length of the radiator with rectangular patch (a) and two L-shaped strips ($l_3 + l_4$ and $l_5 + l_6$) is about quarter wave length. Table 1 shows the final optimized dimensions of the proposed design.

In order to explain the detailed process of improvement for the proposed antenna, three antennas (Ant. 13) are illustrated in Figure 2. Simulated return losses and ARs are displayed in Figure 3. Ant. 1 is

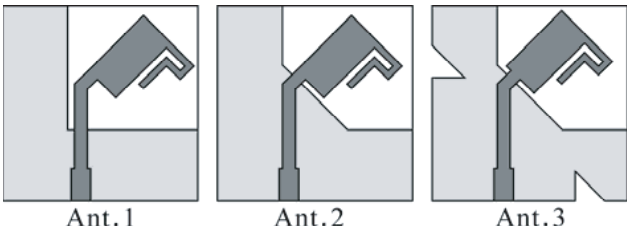

Figure 2. Three improved prototypes of the proposed antenna.

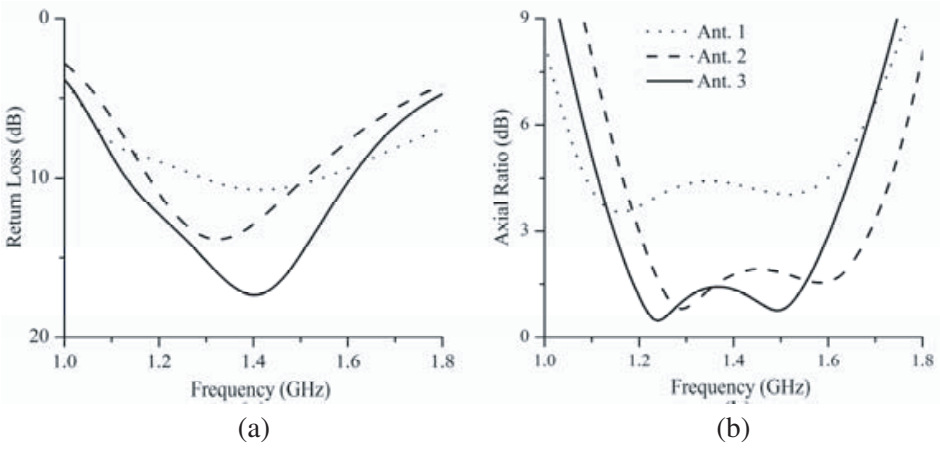

Figure 3. Simulated AR results for Ant. 13. (a) Return loss and (b) AR.

the initial monopole antenna with a radiator and an L-shaped ground plane. By appropriately adjusting the length of the rectangular patch and L-shaped strips, the resonant frequency can be controlled and the impedance match can be improved. As can be seen in Figure 3, simulated results of Ant. 1 indicate that the resonant frequency is at 1.4 GHz but no 3-dB AR bandwidth can be obtained. In order to enlarge the impedance bandwidth and improve the CP performance, an isosceles right triangular perturbation is added to the corner of the L-shaped ground plane. Simulated results of Ant. 2 show that the perturbation provides a great help for the impedance matching and CP excitation. A wide 3-dB AR bandwidth from 1.2 to 1.7 GHz is obtained with 10-dB return loss bandwidth from 1.2–1.47 GHz. To further enlarge the impedance bandwidth and improve the CP operating band to cover the whole GNSS bands, the position of the radiator is optimized and two isosceles right triangular slits are embedded in the left and bottom sides of the ground. Simulated results of Ant. 3 demonstrate that it can provide a wide impedance bandwidth as better impedance matching could be obtained by adjusting the position of the radiator. In addition, by introducing the triangular silts in the ground plane, the required 3-dB AR bandwidth can be achieved as the phase and amplitude of the electric field are improved. Simulated results show that the Ant. 3 provides the 10 dB return loss bandwidth from 1.14 to 1.62 GHz and 3-dB AR bandwidth from 1.14 to 1.61 GHz. In short, it plays a key role in CP improvement by adding the isosceles right triangular perturbation and the two isosceles right triangular slits, while adjusting the position of radiator can improve the impedance matching.

Figure 4 depicts the simulated current distributions with four different phases for the proposed CP antenna at 1.268 GHz to explain the CP mechanism where J_{sum} represents the vector sum of the major current distributions. As shown in Figure 4, J_{sum} is along $+y$ direction at 0° phase and along x direction at 90° phase. It also can be found that the J_{sum} at 180° is orthogonal to the J_{sum} at 270°. The J_{sum} rotates counter clockwise as the time increases, thus generating the right-hand circular polarization (RHCP). In addition, the left-hand circular polarization (LHCP) can be achieved by inverting the radiator and the ground plane.

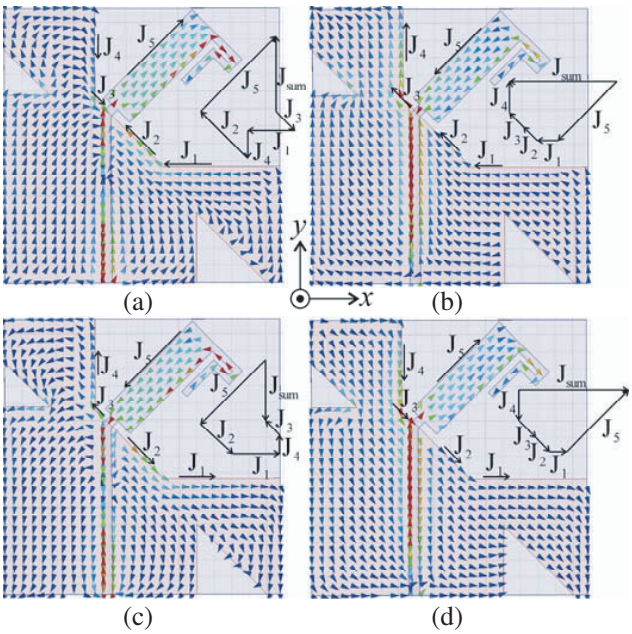

Figure 4. Current distributions of the designed antenna at 1.268 GHz. (a) 0°, (b) 90°, (c) 180°, (d) 270°.

2.2. Parameter Analysis

The effects of the four key parameters ($d_x/t/s_2/s_4$) on impedance and AR bandwidths in the broadside direction are analysed and discussed by using commercial software Ansys High Frequency Structure

Simulator (HFSS) for further study. All the other parameters remain in the optimal values unless stated.

The impacts of position of the radiator and feed line d_x on the proposed CP antenna are depicted in Figure 5. As shown in Figure 5, the return loss tends to shift to the higher frequency as d_x increases. In addition, the variation of d_x has bigger effect for AR performance at lower frequency band than the higher one. Figure 6 shows the effects of the isosceles right triangular perturbation on the proposed design. The length of the perturbation t could significantly affect the impedance matching when it increases, while the AR bandwidth changes slightly. The significant impacts of the width of ground plane s_2 and s_4 are displayed in Figure 7. In this design, the coupling between ground plane and the radiator is a key point to achieve circular polarization. So the size of ground plane plays an important role in controlling the impedance bandwidth and AR As can be seen in Figure 7, the desired 10-dB return loss bandwidth and 3-dB AR bandwidth can be achieved with $s_2 = 26.1$ mm and $s_4 = 33.4$ mm. The performance can be greatly reduced with the decrease of s_2 or s_4. In order to obtain the proper impedance and AR bandwidths, the values of $d_x = 29.4$ mm, $t = 19.5$ mm, $s_2 = 26.1$ mm and $s_4 = 33.4$ mm are selected, respectively.

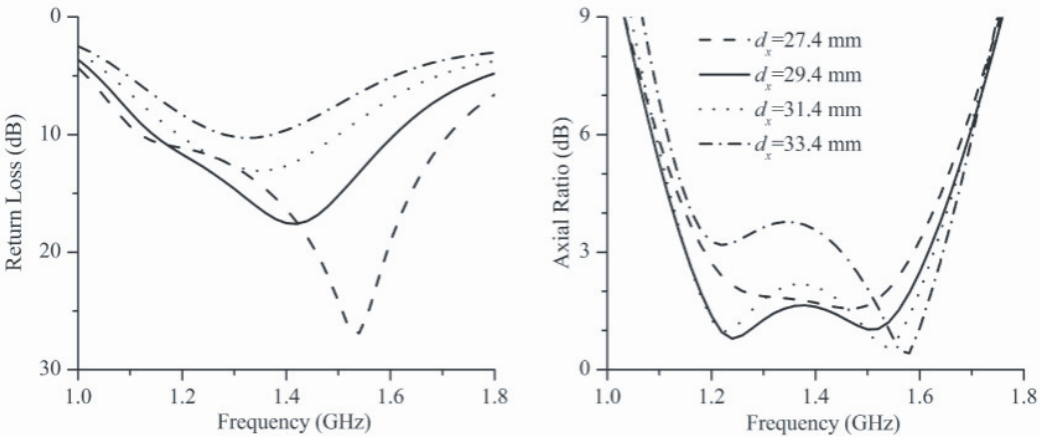

Figure 5. Effect of d_x on antenna performance. (a) Return loss and (b) AR.

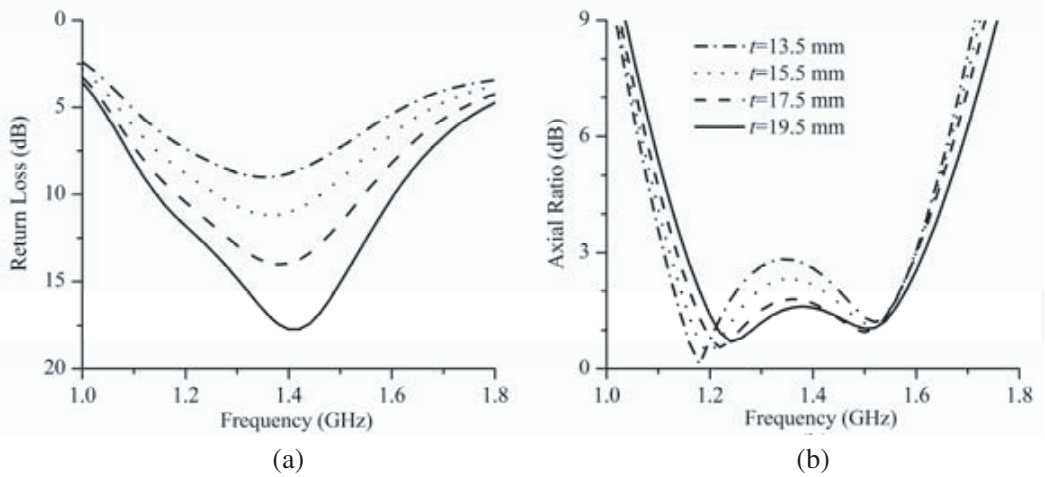

Figure 6. Effect of t on antenna performance. (a) Return loss and (b) AR.

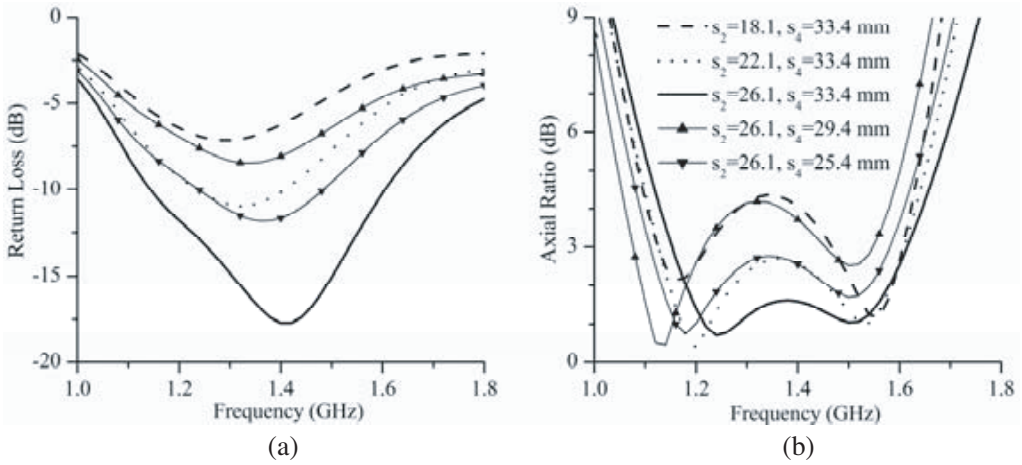

Figure 7. Effect of s_2 and s_4 on antenna performance. (a) Return loss and (b) AR.

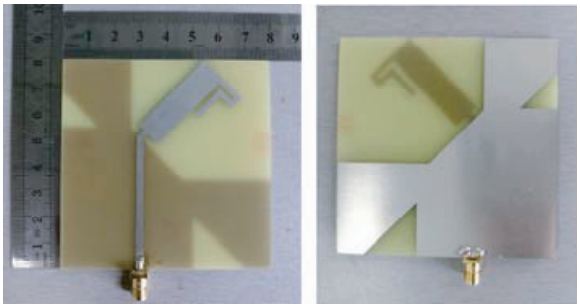

Figure 8. Photographs of the proposed antenna.

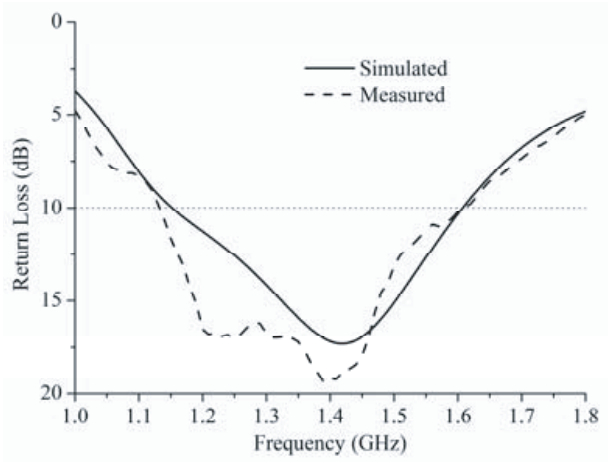

Figure 9. Simulated and measured return loss of the proposed antenna.

3. EXPERIMENTAL RESULTS AND DISCUSSION

A prototype of the proposed antenna was fabricated and tested to verify the feasibility of the broadband CP characteristic, as shown in Figure 8. Figure 9 shows the measured and simulated return loss, which was measured by an Agilent N5247A vector network analyser. The measured 10 dB return loss bandwidth of 35.6% from 1.13 to 1.62 GHz was obtained. Figure 10 displays the measured and simulated ARs in the broadside direction Measured result demonstrates the antenna provides a wide 3-dB AR bandwidth of 35.4% from 1.14 to 1.63 GHz. Figure 11 gives the simulated and measured peak gains of the proposed antenna versus frequency. It can be observed that the measured gain is more than 2.75 dBic for the 3-dB AR band with a maximum value of 4.42 dBic. The measured efficiency of the proposed antenna is shown in Figure 12. Figures 13 and 14 plot the measured and simulated radiation patterns for RHCP and LHCP in *xoz*-plane and *yoz*-plane at 1.268 and 1.561 GHz, respectively. As can be seen, the proposed antenna exhibits RHCP radiation in the $+z$-direction and LHCP radiation in the $-z$-direction. A good agreement has been obtained between simulated and measured results, while the slight discrepancies are mostly attributed to the unstable characteristic, the fabrication tolerances and the welded joint of SMA connector. Table 2 summarizes the AR and gain in the broadside direction of the antenna for different GNSS standards. The performances of the antennas in [17–22] and the proposed antenna are shown in Table 3.

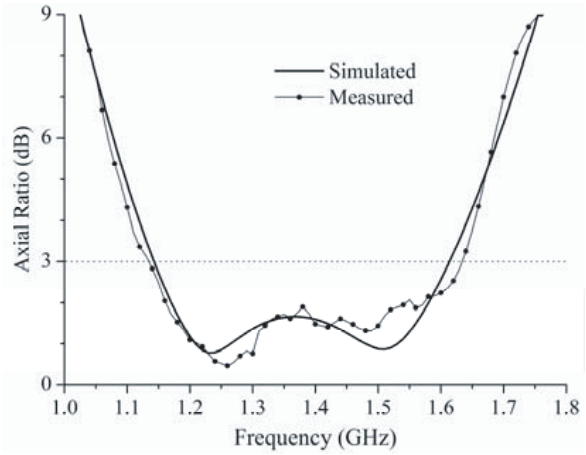

Figure 10. Simulated and measured AR of the proposed antenna.

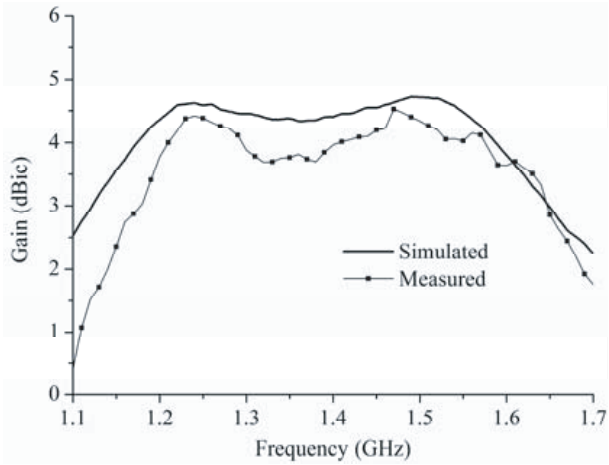

Figure 11. Simulated and measured gain of the proposed antenna.

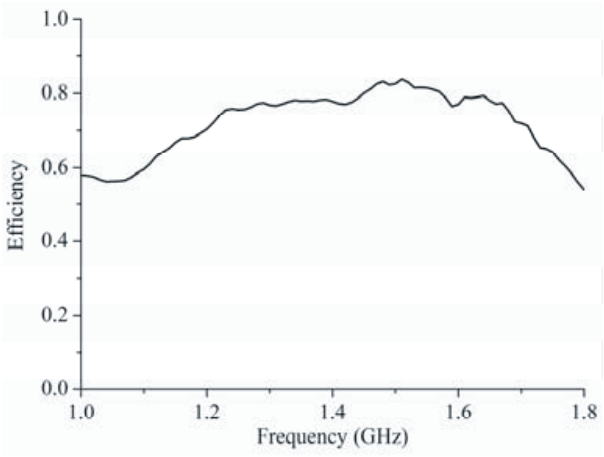

Figure 12. Measurement of efficiency of the proposed antenna.

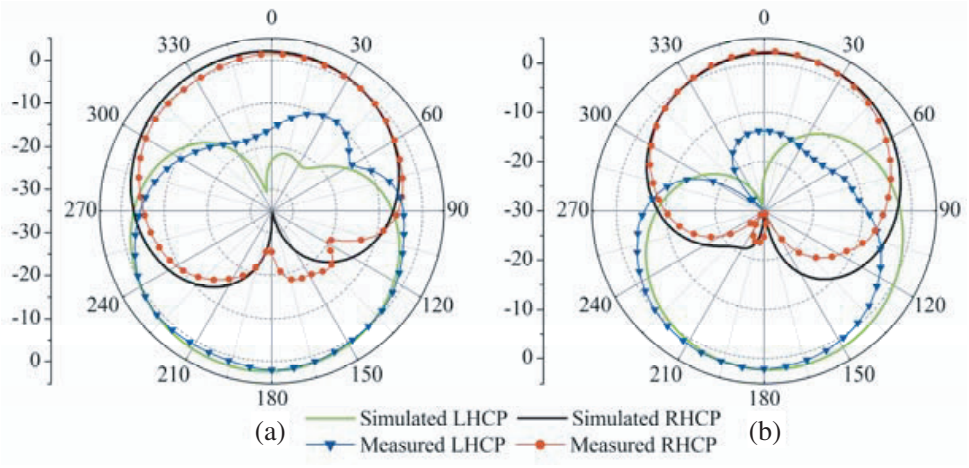

Figure 13. Measured and simulated radiation patterns at 1.268 GHz in (a) *xoz*-plane and (b) *yoz*-plane.

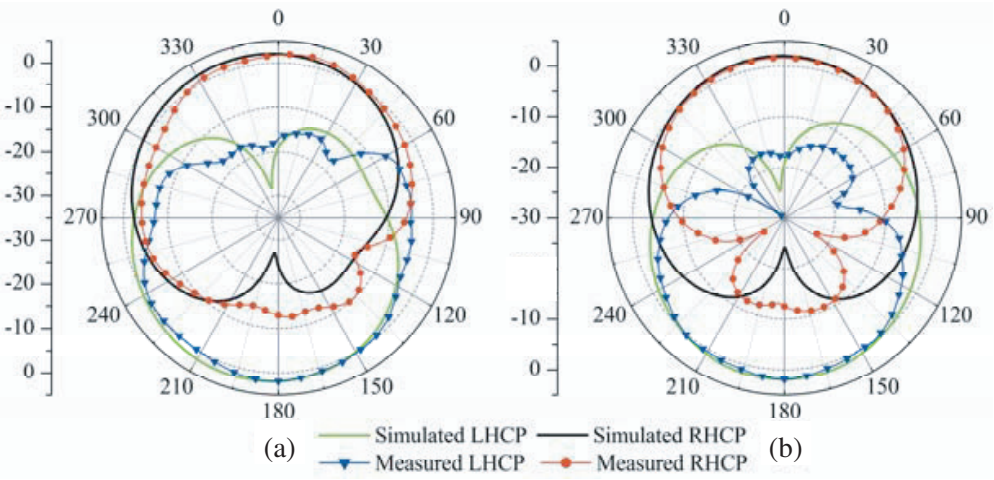

Figure 14. Measured and simulated radiation patterns at 1.561 GHz in (a) *xoz*-plane and (b) *yoz*-plane.

Table 2. AR and gain in broadside direction for the different GNSS standards.

Proposed antenna	GNSS Standards								
	GPS/GLONASS			Galileo			Beidou		
	L_1	L_2	L_5	E_1	E_6	E_5	B_1	B_2	B_3
AR (dB)	<1.93	<0.78	<1.62	<1.93	<0.67	<1.30	<1.88	<1.04	<0.51
Gain (dBic)	>3.88	>4.00	>2.75	>3.88	>4.22	>3.03	>4.12	>3.78	>4.03

Table 3. Comparison of the broadband GNSS CP antennas.

Reference	Antenna size (mm^3)	3-dB ARBWs(%)	Peak gains (dBi)
[17]	$110 \times 110 \times 28$	16	8
[18]	$40 \times 40 \times 6$	2.5	5
[19]	$250 \times 250 \times 50$	38	7.4
[20]	$90 \times 90 \times 51$	23.5	2.8
[21]	$334 \times 334 \times 69$	30.6	7.9
[22]	$60 \times 60 \times 1.6$	21.8	6.6
Proposed	$79 \times 79 \times 1.5$	35.4	2.9

4. CONCLUSION

In this paper, a novel broadband circularly polarized monopole antenna for GNSS applications is designed, analyzed and tested, which is a combination of simple tilted radiator and an improved ground plane. Parameter analysis shows that wide impedance and 3-dB AR bandwidths can be obtained by appropriately adjusting the location of the radiator and the size of the isosceles right triangular perturbation. Measured results show that the total GNSS bands can be covered successfully. Therefore, the proposed antenna is a good candidate for different GNSS applications which require good CP performance and compact size.

REFERENCES

1. Wang, J. J. H., "Antennas for global navigation satellite system (GNSS)," *Proc. IEEE*, Vol. 100, No. 7, 2349–2355, 2012.
2. Guo, J. L., Y. H. Yang, Y. H. Huang, and B. H. Sun, "Slot multi-arm helix antenna with simple and efficient feeding network," *Electron. Lett.*, Vol. 51, No. 16, 1224–1226, 2015.
3. So, K. K., H. Wong, K. M. Luk, and C. H. Chan, "Miniaturized circularly polarized patch antenna with low back radiation for GPS satellite communications," *IEEE Trans. Antennas Propag.*, Vol. 63, No. 12, 5934–5938, 2015.
4. Byun, G., H. Choo, and S. Kim, "Design of a small arc-shaped antenna array with high isolation for applications of controlled reception pattern antennas," *IEEE Trans. Antennas Propag.*, Vol. 64, No. 4, 1542–1546, 2016.
5. Chen, J., K.-F. Tong, A. Al-Armaghany, and J. Wang, "A dual-band dual-polarization slot patch antenna for GPS and Wi-Fi applications," *IEEE Antennas Wireless Propag. Lett.*, Vol. 15, 406–409, 2016.
6. Rezaeieh, S. A., "Dual band dual sense circularly polarised monopole antenna for GPS and WLAN applications," *Electron. Lett.*, Vol. 47, No. 22, 1212–1214, 2011.
7. Cai, Y.-M., K. Li, Y.-Z. Yin, and X. Ren, "Dual-band circularly polarized antenna combining slot and microstripmodes for GPS with HIS ground plane," *IEEE Antennas Wireless Propag. Lett.*, Vol. 14, 1129–1132, 2015.
8. Kang, M. C., G. Byunand, and H. Choo, "Design of a miniaturized dual-band antenna for improved directivity using a dielectric-loaded cavity," *Microwave Opt. Technol. Lett.*, Vol. 57, No. 7, 1591–1595, 2016.
9. Zhang, Y.-Q., X. Li, L. Yang, and S.-X. Gong, "Dual-band circularly polarized annular-ring microstrip antenna for GNSS applications," *IEEE Antennas Wireless Propag. Lett.*, Vol. 12, 615–618, 2013.
10. Sun, C., H. Zheng, L. Zhang, and Y. Liu, "A compact frequency-reconfigurable patch antenna for beidou (COMPASS) navigation system," *IEEE Antennas Wireless Propag. Lett.*, Vol. 13, 967–970, 2014.
11. Pham, N., J.-Y. Chung, and B. Lee, "A proximity-fed antenna for dual-band GPS receiver," *Progress In Electromagnetics Research C*, Vol. 61, 1–8, 2016.
12. Yoon, Y. and B. Lee, "A cavity-backed traveling wave antenna for tri-band GPS applications," *IEEE Antennas Wireless Propag. Lett.*, Vol. 15, 1454–1457, 2016.
13. Liu, Y., D. Shi, S. Zhang, and Y. Gao, "Multiband antenna for satellite navigation system," *IEEE Antennas Wireless Propag. Lett.*, Vol. 15, 1329–1332, 2016.
14. Liao, W.-J., J.-T. Yeh, and S.-H. Chang, "Circularly polarized chip antenna design for GPS reception on handsets," *IEEE Trans. Antennas Propag.*, Vol. 62, No. 7, 3482–3489, 2014.
15. Chen, H.-M., Y.-F. Lin, C.-H. Chen, P.-Y. Pan, and Y.-S. Cai, "Miniature folded patch GPS antenna for vehicle communication devices," *IEEE Trans. Antennas Propag.*, Vol. 63, No. 5, 1891–1898, 2015.
16. Bilgic, M. M. and K. Yegin, "Modified annular ring antenna for GPS and SDARS automotive applications," *IEEE Antennas Wireless Propag. Lett.*, Vol. 15, 1442–1445, 2016.
17. Fu, S., Q. Kong, S. Fang, and Z. Wang, "Broadband circularly polarized microstrip antenna with coplanar parasitic ring slot patch for L-band satellite system application," *IEEE Antennas Wireless Propag. Lett.*, Vol. 13, 943–946, 2014.
18. Long, J. and D. F. Sievenpiper, "A compact broadband dual-polarized patch antenna for satellite communication/navigation applications," *IEEE Antennas Wireless Propag. Lett.*, Vol. 14, 273–276, 2015.
19. Chen, C., X. Zhang, S. Qi, and W. Wu, "Wideband circular polarization cavity-backed slot antenna for GNSS applications," *Progress In Electromagnetics Research Letters*, Vol. 52, 31–36, 2015.

20. Lin, W. and H. Wong, "Wideband circular polarization reconfigurable antenna," *IEEE Trans. Antennas Propag.*, Vol. 63, No. 12, 5938–5944, 2015.
21. Wang, E., Z. Wang, and Z. Chang, "A wideband antenna for global navigation satellite system with reduced multipath effect," *IEEE Antennas Wireless Propag. Lett.*, Vol. 12, 124–127, 2013.
22. Pakkathillam, J. K. and M. Kanagasabai, "Circularly polarized broadband antenna deploying fractal slot geometry," *IEEE Antennas Wireless Propag. Lett.*, Vol. 14, 1286–1289, 2015.